Crystal Calorimeter R&D for the Electron Ion Collider (EIC)

T. Horn, C. Munoz-Camacho, *Member, IEEE*, G. Charles, G. Hull, M. Carmignotto, A. Mkrtchyan, H. Mkrtchyan, C. Woody, *Fellow, IEEE*, S. Stoll,*Member, IEEE*, and R.-Y. Zhu, *Senior Member, IEEE*

***Abstract*—This paper reports on R&D efforts to build a PbWO4-based inner endcap calorimeter for the Electron-Ion Collider exploring the limits of PbWO4 quality. Since the construction of the CMS and early PANDA ECAL the worldwide availability of high quality PbWO4 production has changed dramatically. Studies of crystals from SIC, the remaining manufacturer of crystals, seem to indicate problems maintaining good crystal quality. We report on recent studies of the quality of crystals produced by SICCAS in 2014 including transmittance, light output, and radiation damage effects. We also briefly discus recent progress with CRYTUR as an alternate supplier of PbWO4, as well as readout options and planned prototype studies for the EIC inner endcap calorimeter.**

***Index Terms*—Crystal, light output, photo-luminescence, radiation damage, scintillator, transmission, SiPM, Electron-Ion Collider**

I. Introduction

GAINING a quantitative description of the nature of strongly bound systems is of great importance for our understanding of the fundamental structure and origin of matter. Nuclear science deals with the origin and inner structure of the atom, the nucleus and nucleons (protons and neutrons) in it, which account for essentially all the mass of the visible universe. Nucleons themselves consist of more basic constituents, the quarks bound together by gluons. Such strongly interaction systems are governed by the theory of Quantum Chromo-Dynamics (QCD). The Electron-Ion Collider (EIC) is a new experimental facility that will provide a versatile range of kinematics, beam polarizations and beam species, which is essential to precisely image the sea quarks and gluons in nucleons in nuclei and to explore the new QCD frontier of strong color fields in nuclei and to resolve outstanding questions in understanding nucleons and nuclei on the basis of QCD.

This work was supported in part by the National Science Foundation under Grant PHY-1306227.

T. Horn, M. Carmignotto, and A. Mkrtchyan are with the Department of Physics at Catholic University of America, Washington, DC 20064 USA (e-mail: hornt@cua.edu).

C. Munoz-Camacho, G. Charles, and G. Hull are with the Institut de Physique Nucleaire, Orsay France (e-mail: munoz@jlab.org).

H. Mkrtchyan is with the Alikanyan National Laboratory, Yerevan, Armenia (e-mail: hamlet@jlab.org).

C. Woody and S.Stoll are with the Brookhaven National Laboratory, Upton, NY (email: woody@bnl.gov, stoll@bnl.gov).

R.-Y. Zhu is with Caltech, Pasadena, CA (email: zhu@caltech.edu).

One of the main goals of the EIC is the three-dimensional imaging of nucleon and nuclei and unveiling the role of orbital angular motion of sea quarks and gluons in forming the nucleon spin. These studies are made possible through a new framework developed to explore nucleon structure through the Generalized Parton Distributions (GPDs) and the Transverse Momentum-Dependent parton distributions (TMDs). GPDs can be viewed as spatial densities at different values of the longitudinal momentum of the quark, and due to the space-momentum correlation information encoded in the GPDs, can link through the Ji sum rule to a parton's angular momentum. The TMDs are functions of both the longitudinal and transverse momentum of partons, and offer a momentum tomography of the nucleon complementary to the spatial tomography of GPDs. TMDs can be accessed through semi-inclusive Deep Inelastic Scattering. GPDs can be probed through exclusive reactions, for instance, Deeply Virtual Compton Scattering (DVCS), which is deemed the cleanest process to probe GPDs. Detailed information about the EIC science program can be found in the EIC White Paper [1].

To carry out the scientific program at an EIC, and in particular to precisely determine the GPDs and TMDs, high luminosity, polarized beams, and a specialized detector are needed. The detector design is driven by the requirements of the semi-inclusive and exclusive scattering processes, which require detection of all particles in the reaction with high precision. The specifics of the particle dynamics for each reaction have thus to be taken into account. Details on the detector design considerations can be found in the EIC White Paper [1].

For the measurement of the DVCS process it is important to eliminate or reduce background signals coming from Bethe-Heitler events [2]. This requires good separation of the scattered particles, in particular in the electron-going direction. To satisfy these requirements the Particle Identification (PID) in the electron endcap should provide: 1) good resolution in angle to at least 1 degree to distinguish between clusters, 2) energy resolution to a few %/√E for measurements of the cluster energy, and 3) the ability to withstand radiation down to at least 1 degree with respect to the beam line [1,3,4].

Crystal calorimeters have been used in nuclear and high energy physics for their high resolution and detection efficiency and thus would be the preferable solution for the EIC. In particular, a solution based on $PbWO_4$ would be optimal due to its small Moliere radius and radiation hardness.

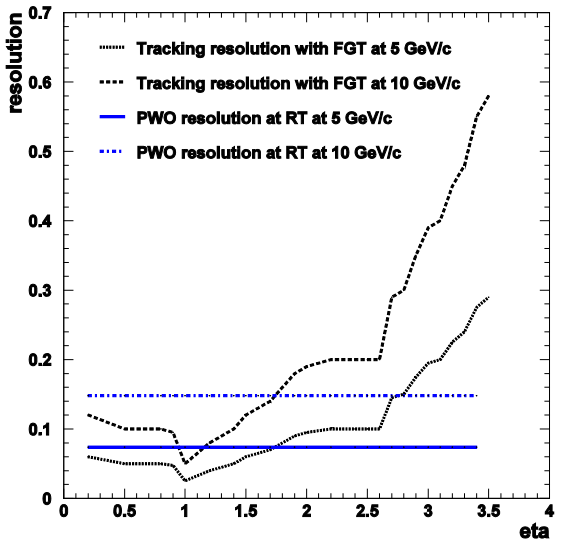

Fig. 1. (color online) The resolution as a function of rapidity (eta) for tracker and PbWO4 crystals at representative particle momenta of 5 GeV/c and 10 GeV/c of the experiments. The tracking resolution at large values of eta is relatively poor and can be compensated by that of high resolution crystals.

PbWO4 has been used for existing calorimeters (CMS, JLab Hall B) and high quality crystals are being considered to be used in several new electromagnetic calorimeter projects around the world (PANDA, JLab 12 GeV). The critical aspect for crystal quality, and thus resolution, is the combination of high light output and radiation hardness, which depend strongly on the manufacturing process. The main goal addressed by the present R&D is to identify what would need to be done to be able to build a PbWO4-based inner endcap calorimeter for the EIC exploring the limits of PbWO4 quality.

II. CALORIMETRY IN THE EIC ELECTRON ENDCAP

In general, electromagnetic calorimetry has two main functions: particle reconstruction, and particle identification (PID). The latter is important for discriminating single photons from, e.g., DVCS and two photons from π^0 decay, and electrons from pions. The reconstruction requirements is driven by the need to accurately reconstruct the four-momentum of scattered electrons at small angles, where the angular information is provided by the tracker, but the momentum (or energy) can come from either the tracker or the EM calorimeter. Since the calorimeter resolution follows the functional form $a/\sqrt{E} + b$, and the tracking resolution goes as $Ap + B/p + C$ (where B is due to multiple scattering), for high electron momenta there will always be a critical angle θ_0, below which the EM calorimeter will, at high momenta in a solenoidal field, provide the better resolution. The tracking resolution for a dedicated EIC detector including a barrel silicon tracker and forward silicon trackers (forward GEM, barrel micromegas) is illustrated as a function of rapidity (angle) in Fig. 1. At large absolute values of the rapidity, η, (both forward and backward) the tracking resolution is poor compared with the resolution of $PbWO_4$ crystals (energy resolution better than 3% at room temperature) for all reasonably high energies. For lower magnetic fields as in, e.g., sPHENIX, the forward tracking resolution would be even lower (gas detector type resolution is ~70 μm vs. while that of silicon is ~20 μm). The energy resolution of $PbWO_4$ can be further improved by cooling the crystals. Resolutions of better than 2% have been achieved at PANDA. For comparison, the energy resolution of lead glass is 5-6%. The best detector resolution at small angles, where the tracking resolution is poor, would thus be achieved by a high-resolution crystal inner part. In general, the resolution of the calorimeter out to a critical distance r_0 and a critical angle θ_0 is given by the sum of the resolution at r_0 and the shower width. PbWO4 has the smallest Moliere radius of all scintillating crystals and is thus the optimal choice. Determining r_0 and θ_0 is part of ongoing studies.

Parameter	Unit	CMS PWO-I	PANDA PWO-II	EIC
Luminescen	nm	420	420	420
ce maximum				
B	magnetic flux density, magnetic induction	1 G → 10^{-4} T = 10^{-4} Wb/m^2		
H	magnetic field strength	1 Oe → $10^3/(4\pi)$ A/m		
m	magnetic moment	1 erg/G = 1 emu → 10^{-3} A·m^2 = 10^{-3} J/T		
M	magnetization	1 erg/(G·cm^3) = 1 emu/cm^3 → 10^3 A/m		
$4\pi M$	magnetization	1 G → $10^3/(4\pi)$ A/m		
σ	specific magnetization	1 erg/(G·g) = 1 emu/g → 1 A·m^2/kg		
j	magnetic dipole moment	1 erg/G = 1 emu → $4\pi \times 10^{-10}$ Wb·m		
J	magnetic polarization	1 erg/(G·cm^3) = 1 emu/cm^3 → $4\pi \times 10^{-4}$ T		
χ_{vol}	susceptibility	1 → 4π		

III. GROWTH AND PRODUCTION OF PWO CRYSTALS

Mass production of PbWO4 was developed by CMS in order to produce the crystals required for use at LHC. During the CMS and early PANDA EMC construction, two manufacturers, BTCP and SIC, using different crystal growth methods were available. Essentially all high quality crystals have been produced at BTCP using the Czochralski growing method, whereas SIC produces crystals using the Bridgman method. BTCP is now out of business, and the worldwide availability of high quality PbWO4 production has changed dramatically. Recent PANDA studies of crystals produced between 2012 and early 2014 by SIC, the remaining manufacturer of crystals, seem to indicate problems maintaining good crystal quality. It is therefore not clear if crystals of the same quality as those produced by BTCP are in fact currently available. The problems might be caused by the Bridgeman technology or details of the manufacturing process at SIC. Therefore, if one needs crystals of very good optical quality, a better approach might be to follow the details of the manufacturing process previously used by BCTP. This process is also used by the company Crytur in the Czech Republic. Crytur has access to the same raw material (i.e., powder) that was used by BCTP including sensible details on the growing process. It would therefore seem likely that they should be able to produce crystals of the same quality and radiation hardness as BCTP did for CMS and within a reasonable time period.

Table 1: crystal specifications

Parameter	Unit	CMS PWO-I	PANDA PWO-II	EIC
Luminescence maximum	nm	420	420	420
Expected energy range of EMC	GeV	0.15-1000	0.01-10	0.1-15
Light Yield at RT	pe/MeV	8	16	15?
EMC operating temperature	℃	+18	-25	
Energy resolution at 1 GeV	%	3.4	2.0	few %/E
LY(100ns)/LY(us)		0.9	0.9	
Transmittance @360nm	%	25	35	
Transmittance @420nm	%	55	60	
Transmittnace@620nm	%	65	70	
Homogeneity at T=50%	nm	3.0	3.0	
Induced absorption coefficient k at RT, >100 Gy/hr	m-1	1.6	1.1	1.5?
Mean value of k	m-1		<0.75	

Based on this current situation, there is a clear need to develop an alternate supplier of PbWO4 if it is to be used for a future EIC crystal calorimeter in parallel with the current efforts. The main goal addressed by the present R&D effort is to identify what would need to be done to be able to build a PbWO4-based endcap calorimeter for the EIC exploring the limits of PbWO4 quality.

IV. EIC Crystal Specifications

Table 1 lists the physical goals and specifications for the PWO crystals for CMS and PANDA, which were used in earlier contracts with BTCP and crystals grown according to the Czochralsky technology. The stricter requirements of PANDA resulted in the development of the "PWO-II" crystals, which featured a 60% lower La and Y doping concentration level compared to "PWO-I" and an increase of a factor or two in light yield. A few initial estimates of ranges for the EIC are shown in the last column. The EIC requirement on radiation hardness may be lower than that of PANDA, but detailed studies have yet to be done. The general question whether the EIC could use more relaxed crystal specs, also in terms of variations, is a key question of our ongoing R&D.

V. Crystal Quality Studies

To test the crystal performance the university lab infrastructure at IPN-Orsay and CUA has been optimized for such tests. Both groups have started setting up the necessary infrastructure to perform crystal quality tests. Using crystals originally manufactured by BTCP (Russia), borrowed from the University of Giessen, transmittance measurements, in both longitudinal and transverse direction with respect to the crystal main axis were performed.

We have used a Varian Cary 5000 spectrometer (Fig. 2, top left) currently available on Campus at the Institute of Molecular Chemistry and Materials of Orsay (ICMMO). This spectrometer can take absorption measurements along and across the crystals with a 1 nm wavelength resolution between 200 and 800 nm. Collimators are installed in front of the beam source in order to produce a clean beam spot. Typically, 4 absorption spectra were measured: three of them transverse to the block at positions and one longitudinal. The spectrometer is calibrated each time a crystal is changed or moved. Transmittance results obtained for a sample crystal are shown in Fig. 2 (top right), for all four positions and as a function of the incident beam wavelength. Transmittance starts around 350 nm and reaches values close to 90% at higher wavelengths.

The group at CUA has access to a Perkin-Elmer Lambda 750 photo-spectrometer through the Vitreous State Laboratory on campus. The spectrometer allows for measurements of the transmittance and absorption between wavelengths of 200 to 900 nm with 1 nm resolution. The spectrometer compartment

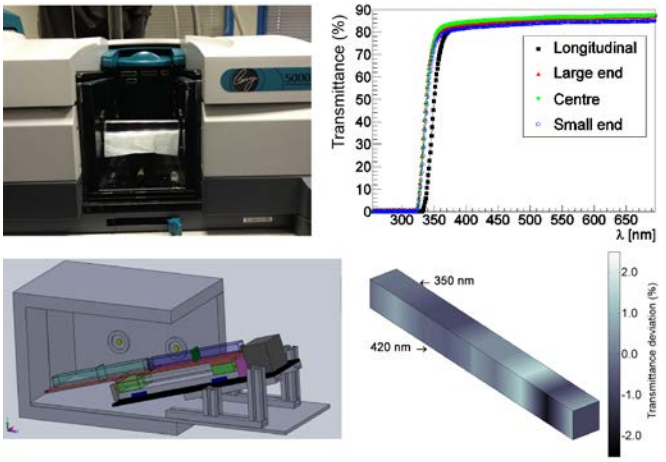

Fig. 2. (color online) (top left) The optical transmittance is measured using a photospectrometer (Varian at IPNO and Perkin-Elmer at CUA); (top right) example of a crystal transmittance spectrum; (bottom left) modified spectrometer compartment to accommodate long crystals; (bottom right) example of transmittance variation along the crystal

is optimized for characterizing 1-cm long liquid glass samples and had to be modified for testing 20-cm long crystal samples. The modified compartment will be equipped with a horizontal positioning slide and a programmable stepper motor. The assembly is arranged at an angle of about 15 degrees to avoid interference of the reference beam with the crystal itself as shown in Fig. 2 (bottom left). This setup still allows for transmittance measurements at normal incidence angles.

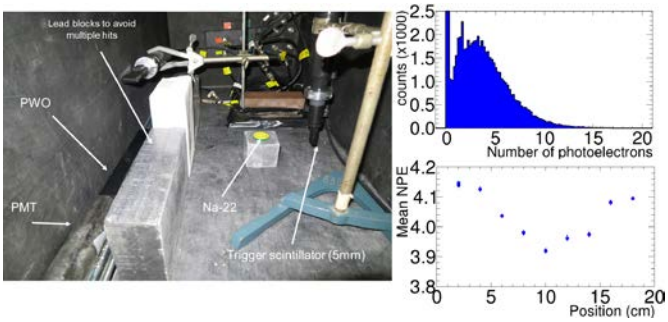

Fig. 3. (color online) The light yield of the crystal is measured using a radioactive source. (right top) Representative ADC spectrum including the pedestal showing the light yield determined using 22 Na; (right bottom)the light yield along the crystal varies by about 4%, which could be due to temperature fluctuations between data points.

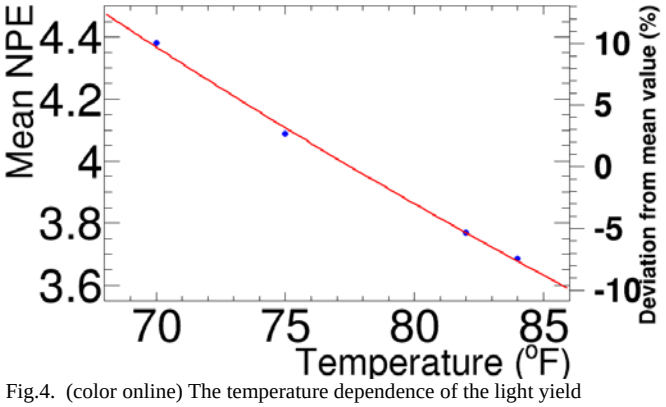

Fig.4. (color online) The temperature dependence of the light yield

A light yield measurement setup based on radioactive sources is shown in Fig. 3. The crystals were wrapped in a layer of enhanced specular reflector and optically coupled to the entrance window of a 2" photomultiplier (Hamamatsu R1924A). The anode signal are directly digitized using a charge sensitive ADC (LeCroy 2249A). The light yield shown in Fig. 3 was determined using a ^{22}Na source, where photons of 511 keV are emitted from e^-e^+ annihilation. In separate measurements the response to a single photoelectron has been determined to calibrate the signal amplitude above the pedestal in units of photoelectrons. A representative ADC spectrum is shown in the right top panel in Fig. 3. Also shown is the measured light yield at 27°C along the crystal, which varies on the level of about 4%. This may be due to fluctuations in the temperature between data points. No attempt was made to stabilize the temperature during the measurements. Fig. 4 shows a dependence of the light yield on the temperature of 2.4%/°C. This is consistent with previous measurements published in Ref. [5]. To control this systematic effect options for operating the setup in a temperature controlled environment are being explored.

A. Optical Properties of 2014/15 SIC Crystals

One of the currently most representative sets of PWO crystals manufactured by SIC has been measured for optical properties at JLab. The data were taken with a setup consisting of a halogen lamp, integrating sphere, holder table for the crystals and optics. The reproducibility of the transmittance measurements with this setup is on the order of a few percent dominated by uncertainties in positioning the crystal. The longitudinal transmittance results for 5 crystals produced by SIC in spring 2014 and 5 crystals produced in December 2014 are shown in Fig. 5. The longitudinal transmittance varies between 60% and 70% for most crystals at a wavelength of 420 nm. One of the crystals shows a completely different behavior above 480 nm compared to the other crystals. The transmittance in the transverse direction (2 cm thickness) was

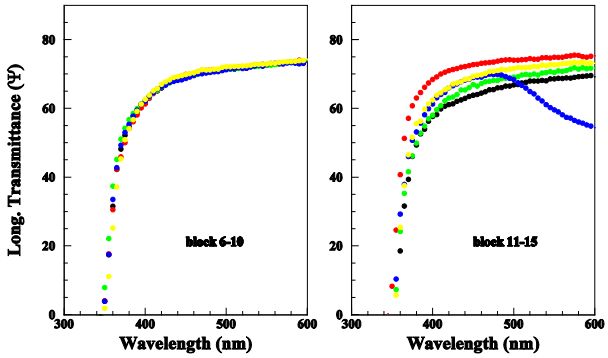

Fig. 5. (color online) Longitudinal transmittance for 10 crystals produced by SIC in 2014. l Crystals #6-#10 were produced in spring and crystals $11-15 were produced in December 2014. The yellow curves in the figures denote crystal #10, and 15. The red curves denote crystal #7, and 12. The black curves denote crystal #6, and 11. The green curves denote crystal #8, and 13. The blue curves denote crystal #9, and 14.

measured at several distances ranging between 5 and 55 mm from the face of the crystal. The results for ten of the fifteen

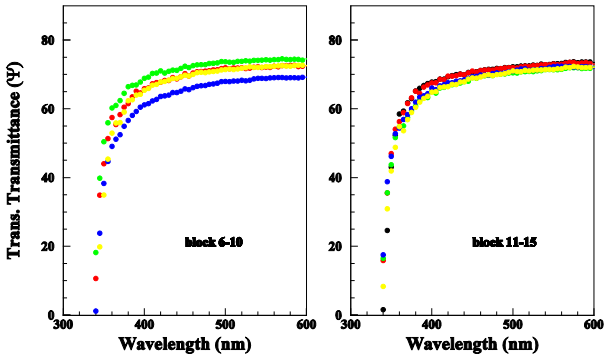

Fig. 6. (color online) Transverse transmittance at 15 mm from the front face for 10 crystals produced by SIC in 2014. l Crystals #6-#10 were produced in spring and crystals $11-15 were produced in December 2014. The yellow curves in the figures denote crystal #10, and 15. The red curves denote crystal #7, and 12. The black curves denote crystal #6, and 11. The green curves denote crystal #8, and 13. The blue curves denote crystal #9, and 14.

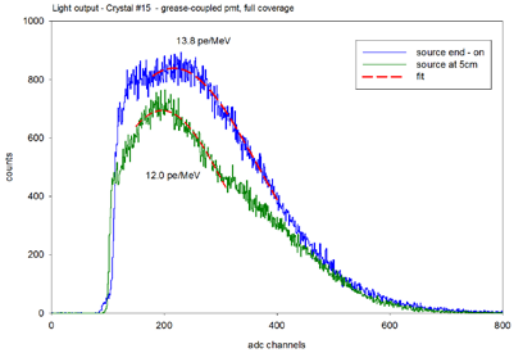

Fig. 7. (color online) Representative ADC spectrum used for calibration. The measurement was carried out at BNL.

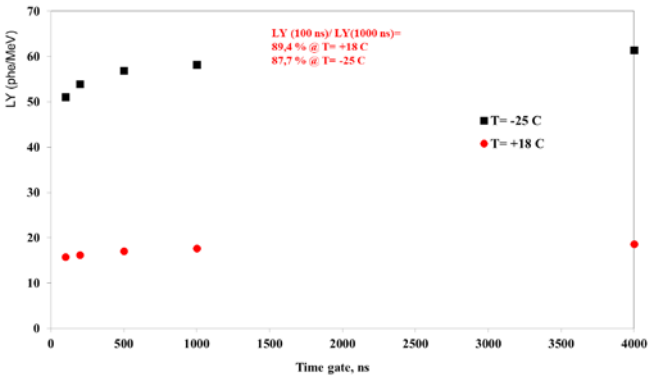

Fig. 9. (color online) The light yield of one of the 2014 SIC produced crystals measured at two temperatures with the setup at Giessen.

crystals at 15 mm from the face of the crystal are shown in Fig. 6. The crystal-to-crystal variation of the transverse transmittance seems to be much less than what was observed for the longitudinal transmission. However, the transmittance of one of the crystals is significantly lower than that of the other crystals.

The crystal light yield was measured for a subset of the fifteen crystals. To calibrate the signal amplitude above the pedestal in units of photoelectrons the response to a single photoelectron (p.e.) has been determined. A representative ADC spectrum is shown in Fig. 7. The light yield response for a subset of crystals at room temperature is shown in Fig 8. The mean of the LO distribution is on the order of 17 photoelectrons/MeV though some of the crystals show a lower yield (see Fig. 8 (right)). Note that the number of

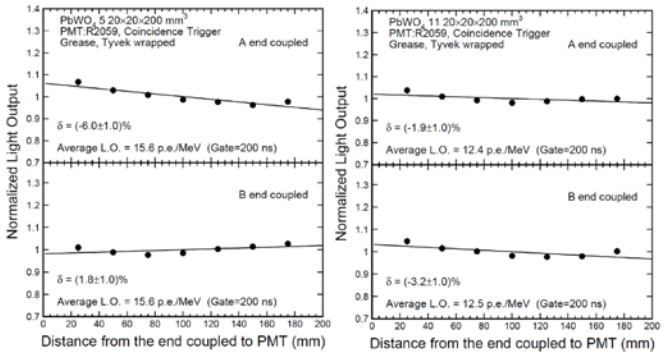

Fig. 8. The light yield of a subset of two crystals measured at Caltech. The number of photoelectrons depends on the quantum efficiency of the PMTs.

photoelectrons depends on the quantum efficiency of the PMTs as discussed in Ref.[6]. Fig. 9 illustrates the change of the light yield over a temperature range of 43 °C starting at +18 °C down to -25 °C. The light yield is shown as a function of the integration gate, which can be used to evaluate the relative contribution of slow components. If such slow components contribute significantly an increase in the relative light yield beyond 1000 ns should be clearly visible. The light yield increases by a factor of about three due to cooling to -25 °C independent of the integration time window.

As shown in Fig. 10 (left) for a subset of two crystals, the optical transmittance seems consistent with CMS quality standards as published in Ref. [7] and is relatively uniform along the crystals. However, there is a global variation from crystal to crystal on the order of 20% as determined from the standard deviation of the LO distribution for seven crystals. The light yield of the crystals also seems to be consistent with CMS quality standards (see Fig. 10 right). Evaluating the variation from crystal to crystal and determining what is acceptable for the EIC inner endcap calorimeter is one of the main goals of the present R&D project.

Understanding the effect of systematic effects on the optical measurements is important for the interpretation of crystal quality. Crystals #5 and #11 were evaluated at Caltech, crystals #7 and #15 were sent to BNL, and crystals #2, 3, 6, 8, and 9 were evaluated at Giessen University. Preliminary results from Caltech suggest that the measured values of the transmittance are *higher* than those shown in Fig. 5 for the JLab measurement. Preliminary results from measurements at Giessen and BNL show similar features in that the measured values of the transmittance are *lower* than those shown in Fig. 5 for the JLab measurement. On average the values are lower by 10-15% though for crystal #2 the difference is more than three times as much. It is interesting to note that there seems to be a significant difference in the shape of the distribution between the JLab and Giessen measurements in the region around 400 nm as illustrated in Fig. 11. Preliminary results of

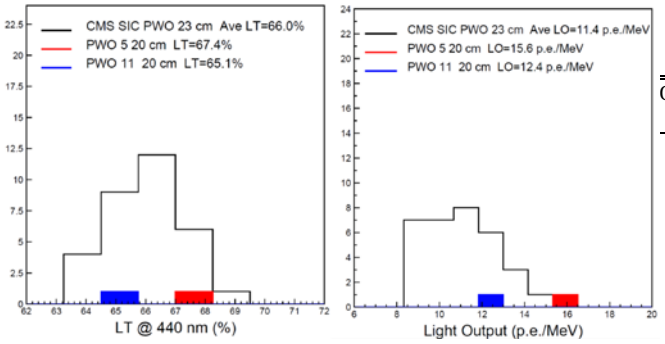

Fig. 10. (color online) Comparison of the optical transmittance and light output of a subset of two crystals to the average quality of CMS crystals.

the light output measurements of crystal #2 at Giessen

Parameter	Unit	CMS PWO-I	PANDA PWO-II
Emission max	nm	420	420
B	magnetic flux density, magnetic induction	1 G → 10^{-4} T = 10^{-4} Vs/m²	
H	magnetic field strength	1 Oe → $10^3/(4\pi)$ A/m	
m	magnetic moment	1 erg/G = 1 emu → 10^{-3} A·m² = 10^{-3} J/T	
M	magnetization	1 erg/(G·cm³) = 1 emu/cm³ → 10^3 A/m	
$4\pi M$	magnetization	1 G → $10^3/(4\pi)$ A/m	
σ	specific magnetization	1 erg/(G·g) = 1 emu/g → 1 A·m²/kg	
j	magnetic dipole moment	1 erg/G = 1 emu → $4\pi \times 10^{-10}$ Wb·m	

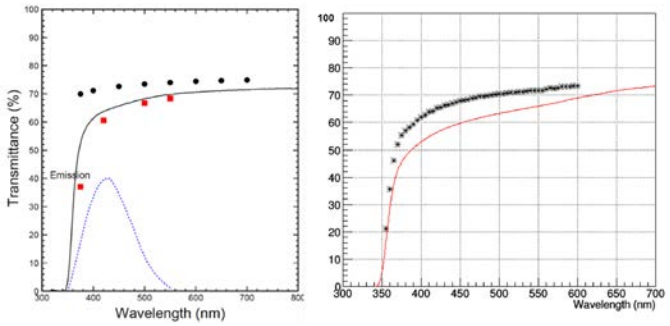

Fig. 11. (color online) Comparison of longitudinal transmittance measurements of the same crystals performed at different facilities: (left) Caltech and JLab denoted by the black solid line and the red points; (right) Giessen (red solid line) and JLab (black points). The measurements at Caltech were performed with a Perkin-Elmer Lambda 950 and at Giessen with a Varian Cary 4000 spectrometer.

University show a value consistent with CMS standards while no clearly interpretable result could be determined for crystal #3. Preliminary results of the absorption coefficient show that four out of five crystals would pass the crystal specification in Table 1. Studies to understand these results and any setup dependent systematic effects are ongoing.

B. Radiation Damage Effects in 2014/15 SIC Crystals

To study crystal radiation damage effects we carried out irradiation tests with electron beams in February 2015 at the Idaho Accelerator Facility, which features a 20 MeV electron beam with 100 Hz repetition rate, with I_{peak}=111 mA (11.1 nC per pulse) and 100 ns pulse width. The beam is roughly 1 mm in diameter and exits through (1/1000)-in thick Ti window, a $x/X_0 = 7.1 \cdot 10^{-4}$ radiation length. Beam position and profile were measured by shooting a glass plate. Scanning the plates and fitting the intensity distribution provides a quantitative (though approximate) measurement of the position and size of the beam at the location of the plate. The front plate was placed at the position of the PbWO4 crystal front faces during irradiation that is 10.75 cm from the beam exit window. The rear plate was located at 33 cm from the beam exit, and shows the beam profile expansion. This provides a relatively homogeneous irradiation and heat load on the crystals. The beam profile is shown in Fig. 12. A $PbWO_4$ crystal at the above mentioned beam parameters will receive a dose of 216 krad/min. Since such radiation dose rate is much higher (~13 Mrad/h) than the dose rates expected during the actual experiments, our tests were carried out at lower dose rates at a reduced accelerator repetition rate, keeping the beam current per pulse and pulse width unchanged. The measured difference of the crystal transmittance before and after irradiation is illustrated in Fig. 13. All transmittance measurements at the Idaho facility were carried out using an OCEAN OPTICS USB4000 device instead of a permanent spectrometer setup. The reproducibility of measurements with this setup ranges from 5% to 15%. The transmittance of some of crystals changed more than 15% after an accumulated dose of 432 krad (at a dose rate of 1.3 Mrad/h), while others do not

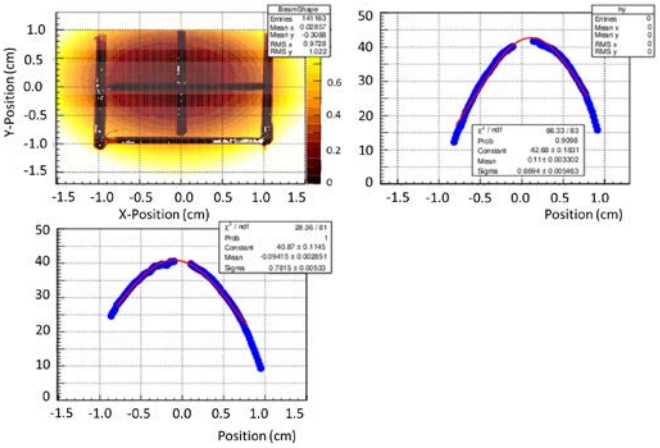

Fig. 12. (color online) *Front (top) profile of the beam at the beginning of test at the Idaho Accelerator Facility. Front plate was located at 33cm from the beam exit (σ_x ~ 0.8 cm, σ_y ~ 0.7 cm),*

seem to show any effects of radiation damage. The change in transmittance for positions far from the front of crystals decreases with the distance. The effect of radiation damage is in part spontaneously recovered after a time period of 60 hours. Overall the results seem to suggest that the crystals can handle high doses at high dose rates. This is in contrast to earlier results of crystal tests [8] produced during a similar time frame and presumably under the same conditions.

One of the challenges in irradiation studies with beam is

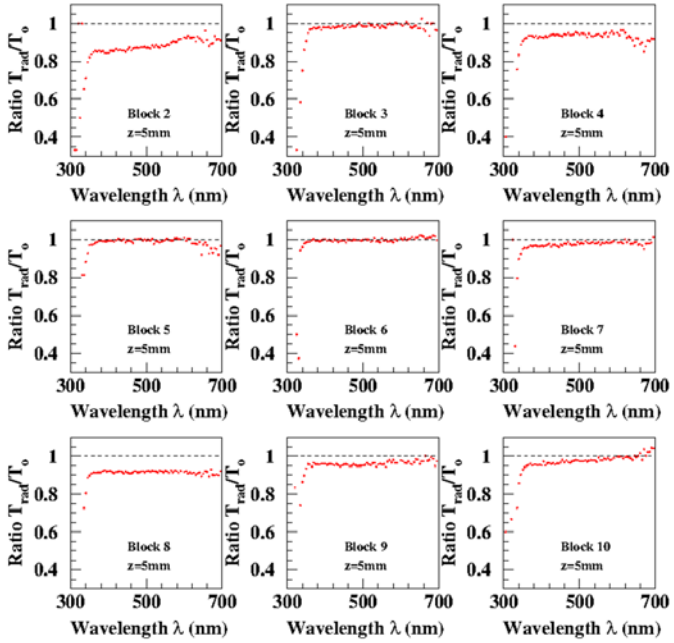

Fig. 13. (color online) *Transmission degradation of the $PbWO_4$ blocks after 432 krad accumulated dose at dose rates of 1.3 Mrad/h. Ratio of transmissions after and before irradiation reflects the level of crystal degradation. For example, crystal #6 shown in the center panel was not damaged significantly.*

temperature control. Ideally one would control the temperature variation during the irradiation measurement within a few percent. This is difficult to achieve when working with an intense and narrowly focused beams, which give a high and

Parameter	Unit	CMS PWO-I	PANDA PWO-II
Luminescen ce maximum	nm	420	420
B	magnetic flux density, magnetic induction	$1\ \mathrm{G} \rightarrow 10^{-4}\ \mathrm{T} = 10^{-4}$ Wb/m^2	
H	magnetic field strength	$1\ \mathrm{Oe} \rightarrow 10^3/(4\pi)$ A/m	
m	magnetic moment	$1\ \mathrm{erg/G} = 1\ \mathrm{emu} \rightarrow 10^{-3}\ \mathrm{A \cdot m^2} = 10^{-3}$ J/T	
M	magnetization	$1\ \mathrm{erg/(G \cdot cm^3)} = 1\ \mathrm{emu/cm^3} \rightarrow 10^3$ A/m	
$4\pi M$	magnetization	$1\ \mathrm{G} \rightarrow 10^3/(4\pi)$ A/m	
σ	specific magnetization	$1\ \mathrm{erg/(G \cdot g)} = 1\ \mathrm{emu/g} \rightarrow 1\ \mathrm{A \cdot m^2/kg}$	

concentrated dose to the crystals, and can even result in heating and thermal damage. As an example, for irradiation at a dose rate of 1.3 Mrad/hr, the temperature near the face of the crystal ramped up at a rate of 0.5 °C/minute. For irradiation at a dose rate of 2.6 Mrad/hr, a rise of the temperature of more than 2°C/minute resulted in severe structural damage to the crystal after 10 minutes. To reach higher doses crystals thus needed to be allowed to cool down between exposures.

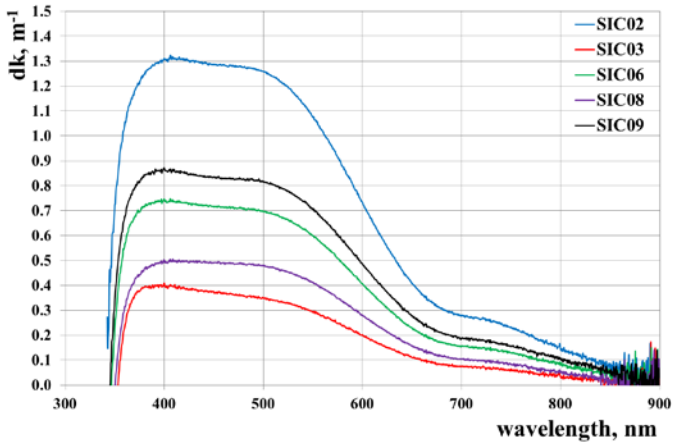

Fig. 14. (color online) Impact of radiation damage in terms of the change of the optical absorption coefficient k as defined in equation 1 for an integral dose of 30 Gy. The absorption coefficient is shown as a function of wavelength over the entire spectrum.

Another challenge in this measurement of radiation damage effects is to minimize surface effects. Ideally, one would measure the same spot before and after radiation minimizing surface effects in the path. Care was taken to ensure that this condition was satisfied and the flat distributions in Fig. 13 seem to suggest that our setup satisfied this condition. To minimize the systematic uncertainty due to recovery of color centers with extremely fast relaxation times our measurements we carried out the transmittance measurement 10 minutes after irradiation. While we could control many of the systematic effects on the measurement it is important to confirm our results and quantify any setup dependent effects. For instance, it is known that there are strong dose rate dependent effects in crystals and their performance under the extreme conditions of our beam tests may be different than at lower dose rates. In general, lower dose rates are more representative of what one would expect in an experiment. The preliminary results of radiation hardness tests of a subset of crystals at Giessen University are shown in Fig 14. The optical transmittance was determined before and after gamma irradiation with an integral dose of 30 Gy imposed within an irradiation period of about 15 minutes. The crystals are kept light tight during and after irradiation until the transmittance measurement is performed exactly 30 minutes at the end of the irradiation. The measurements were performed at room temperature. Fig. 14 quantifies the impact of radiation effects in terms of the change in the absorption coefficient, *k*, which is determined from the longitudinal transmittance spectra before and after irradiation using,

$$dk = \left[\ln\left(T_0 / T_{rad}\right)\right] / d \,, \qquad (1)$$

where T_0 and T_{rad} are the measured transmittance before and after irradiation and d is the total crystal length. The change in k is shown over the entire spectrum of wavelengths in units of m^{-1}.

C. *Status at CRYTUR*

CRYTUR has produced the first 200mm long crystal in rectangular shape (2x2x20cm**3). The crystal was grown making use of pre-production crystals from BTCP as raw material. The crystal has been cut into a rectangular shape, which allows for most efficient investigations of homogeneity, and all surfaces have been polished. The crystal shows a longitudinal non-uniformity of macro defects, which may be due to improper temperature control of the melt during the crystal growth process. The results of the first optical transmittance and radiation hardness properties have been carried out at Giessen University. As shown in Fig. 15 the transmittance of the crystal grown at Crytur falls within 8% of the BTCP crystal at 420 nm. The induced absorption

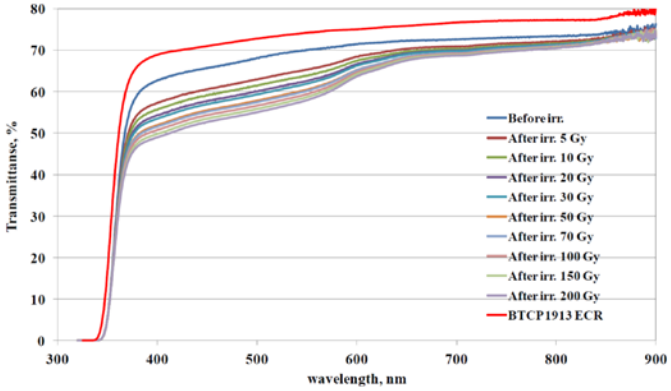

Fig. 15. (color online) Optical transmittance of the full-size Crytur crystal before and after irradiation compared to that of a BTCP crystal.

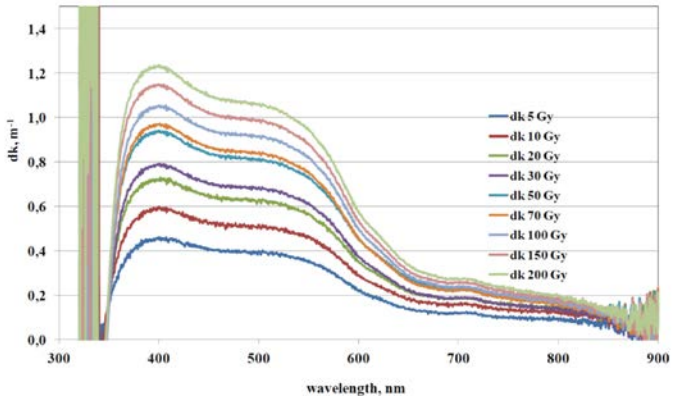

Fig. 16. (color online) Change in induced absorption coefficient of the Crytur crystal for integral doses up to 200 Gy. The crystal is radiation hard.

coefficient up to integral doses of 150 Gy (see Fig. 16), as well as the transmittance at luminescence maximum is consistent with the strict PANDA crystal specifications shown in Table 1.

Parameter	Unit	CMS PWO-I	PANDA PWO-II	EIC

Fig. 17. (color online) Neutral Particle Spectrometer (NPS) prototype produced with 3D printing technology.

D. Readout and Prototype Construction

One of the options to measure the light output of the various $PbWO_4$ crystals is using silicon photomultipliers (SiPMs). These would be ideal photo sensors for reading out the crystals since they produce high gain (~ $3x10^5$) and work inside a magnetic field, given that the EIC forward endcap calorimeter would sit inside the fringe field of a solenoid magnet. At BNL we have carried out initial tests of readout with SiPMs. A setup was constructed with 4 SiPMs coupled to the same crystal. The SiPMs cover about 10% of the corresponding area of a PMT. Measurements with a Cs-137 source showed an energy deposition of 662 keV, which corresponds to about 1 photoelectron. The small size of the signal complicates these measurements and we are exploring alternative techniques to improve the setup. It appears the line spacing of the text changed for the section above

Assuming that our PbWO4 crystal studies continue successfully, another main goal for the next period is to build a small prototype detector consisting of a 5x5 matrix of the new improved crystals. This would allow us to study these crystals in test beam and measure the actual energy and position resolution that we could achieve with them. Further, the prototype would allow us to test a SiPM-based readout system for the crystal inner calorimeter. These measurements would provide additional important information on crystal specifications and their impact on EIC detector performance.

The prototype setup could be based on that for the JLab Neutral Particle Spectrometer (NPS) shown in Fig. 17, which has an active area of about 6x6 cm^2 including a crystal matrix of $PbWO_4$ (and PbF_2 to test hybrid configurations of crystals) in a copper frame. A first version of this prototype was recently constructed at JLab using 3D printing technology. The readout is done by 19 mm Hamamatsu R4125 PMTs with a JLab developed new active HV base.

VI. SUMMARY AND OUTLOOK

A high resolution inner endcap calorimeter in the electron going direction will be an essential piece of equipment at the EIC. This instrument enables precise measurements of DVCS, the method of choice in the program of the three-dimensional imaging of nucleon and nuclei and unveiling the role of orbital angular motion of sea quarks and gluons in forming the nucleon spin. To satisfy the experimental requirements the Particle Identification (PID) in the electron endcap should provide: 1) good resolution in angle to at least 1 degree to distinguish between clusters, 2) energy resolution to a few %/√E for measurements of the cluster energy, and 3) the ability to withstand radiation down to at least 1 degree with respect to the beam line. A solution based on $PbWO_4$ would provide the optimal combination of resolution and shower width at small angles where the resolution of the tracker is poor.

Since the construction of the CMS ECAL and the early construction of the PANDA ECAL the global availability of high quality PbWO4 crystals has changed dramatically. Studies of crystals produced between 2012 and early 2014 by SIC, the remaining manufacturer of crystals, seem to indicate problems maintaining good crystal quality. Our studies of a set of fifteen crystals produced by SIC in 2014 seem to indicate that the overall quality has improved and mostly conform to PANDA requirements. However, a quantitative analysis of the homogeneity of the crystals has yet to be done to fully characterize the crystal quality achievable. Crytur is an alternate vendor for PbWO4 production. The characterization of the first full-size crystal suggests that it conforms to all optical requirements and is radiation hard. Crystal-to-crystal variation remains to be investigated. Assuming that our crystal quality tests are completed successfully and one or two vendors capable of producing such crystals have been identified, the crystal calorimeter R&D will focus in subsequent years on the optimization of geometry, temperature stabilization, cooling and choices of readout system of the endcap inner crystal calorimeter.

Parameter	Unit	CMS PWO-I	PANDA PWO-II	EIC
Luminescen ce	nm	420	420	420
Emission				

B	magnetic flux density, magnetic induction	1 G → 10^{-4} T = 10^{-4} Wb/m^2
H	magnetic field strength	1 Oe → $10^3/(4\pi)$ A/m
m	magnetic moment	1 erg/G = 1 emu

ACKNOWLEDGMENT

This work was supported in part by NSF grant PHY-1306227, Jefferson Laboratory, IPN-Orsay, and the Generic Detector R&D for an Electron-Ion Collider (eRD1). The authors would like to thank Prof. R. Novotny and V. Dormenev for access to data and many helpful discussions.

REFERENCES

[1] A. Accardi et al., "Electron-Ion Collider: The Next QCD Frontier – understanding the glue that binds us all", arXiv.1212.1701, BNL-98815-2012, JLAB-PHY-12-1652 (2012)

[2] EIC Calorimeter Consortium Proposal (April 2012), EIC R&D 1,[ONLINE].Available: https://wiki.bnl.gov/conferences/index.php/Proposals-April2012

[3] D. Boer et al., "Gluons and the sea quarks at high energies", arXiv.1108.1713, BNL-96164-2011, JLAB-PHY-11-1373 (2011)

[4] S. Abeyratne et al., "Science Requirements and Conceptual Design for a Polarized Medium Energy Electron-Ion Collider at Jefferson Lab", arXiv.1209.0775 (2012).

[5] Semenov et al. NIMA 582 (2007) 575-580; R. Mao et al., IEEE Trans. Nucl. Sci. Vol. 55 (2008) 2425-2431.

[6] F. Yang et al., IEEE Trans. Nucl. Sci. Vol. 60 (2013) 2336-2342.

[7] R. Mao et al., IEEE Trans. Nucl. Sci., Vol. 51, No. 4, (2004) 1777.

[8] V. Dormenev et al., Comparison of Radiation Damage Effects in PWO Crystals under 150 MeV and 24 GeV High Fluence Proton Irradiation, IEEE Trans. on Nucl. Sci. Vol 61, No. **1**, 2014, 501-506